

Predictive Deployment of UAV Base Stations in Wireless Networks: Machine Learning Meets Contract Theory

Qianqian Zhang¹, Walid Saad¹, Mehdi Bennis², Xing Lu³, Mérouane Debbah^{4,5},
and Wangda Zuo³

¹Bradley Department of Electrical and Computer Engineering, Virginia Tech, VA, USA, Emails: {qqz93,walids}@vt.edu

²Center for Wireless Communications-CWC, University of Oulu, Finland, Email: mehdi.bennis@oulu.fi

³Department of Civil, Environmental and Architectural Engineering, University of Colorado Boulder, CO, USA, Email: {xing.lu-1,wangda.zuo}@colorado.edu

⁴Mathematical and Algorithmic Sciences Lab, Huawei France R&D, Paris, France, Email: merouane.debbah@huawei.com

⁵Large Systems and Networks Group (LANEAS), CentraleSupélec, Université Paris-Saclay, Gif-sur-Yvette, France

Abstract

In this paper, a novel framework is proposed to enable a predictive deployment of unmanned aerial vehicles (UAVs) as temporary flying base stations (BSs) to complement ground cellular systems in face of downlink traffic overload. First, a novel learning approach, based on the weighted expectation maximization (WEM) algorithm, is proposed to estimate the user distribution and the downlink traffic demand. Next, to guarantee a truthful information exchange between the BS and UAV operators, using the framework of contract theory, a traffic offload contract is developed, and the sufficient and necessary conditions for having a feasible contract are analytically derived. Subsequently, an optimization problem is formulated to deploy an optimal UAV onto the hotspot area in a way that the utilities of the overloaded ground BSs are maximized. Simulation and analytical results show that the proposed WEM approach yields a prediction error which is lower than 12%, and compared with a conventional expectation maximization approach, the WEM method yields a significant advantage on the prediction accuracy, as the traffic load in the cellular system becomes spatially uneven. Furthermore, compared with a baseline, event-driven allocation method, the proposed predictive deployment approach enables UAV operators to provide efficient downlink service for hotspot users, and improves the revenues of both the BS and UAV network operators significantly.

Index Terms – cellular networks; UAV deployment; traffic prediction; contract theory.

I. INTRODUCTION

The use of unmanned aerial vehicles (UAVs) as flying base stations (BSs) has attracted growing interest in the past few years [1]–[8]. Flying UAV BSs can be deployed to complement the

A preliminary version of this work appears in the proceedings of IEEE GLOBECOM 2018 [1].

existing cellular systems, by providing reliable uplink and downlink services for ground users, to potentially increase the network capacity, eliminate coverage holes, and cope with the steep surge of communication needs in hotspot areas [1], [2]. Compared with the terrestrial BSs that are deployed at a fixed location for a long term, UAVs can rapidly change their positions to provide temporary on-demand service [3]. For instance, UAV BSs can be deployed to serve major events (e.g. sport or musical events) during which the terrestrial network capacity is often strained, or to provide communication capabilities for disaster areas in which the ground cellular systems are damaged and cannot provide regular service [4]. Furthermore, UAVs can adjust their positions and establish line-of-sight (LOS) communication links towards ground users, thus improving network performance [5]. Due to the broad range of application domains and their low cost, UAVs as flying BSs is a promising solution to provide temporary connectivity for ground users [6].

However, the deployment of UAVs to provide on-demand cellular service faces several key challenges. For instance, flying UAV BSs are strictly constrained by their on-board energy, which should be efficiently used for communication. However, the on-demand deployment requires UAVs to continuously change their positions to meet instant communication requests. Therefore, most of on-board energy can be consumed by mobility, thus limiting their communication capabilities [1]. Furthermore, to effectively alleviate network congestion during the hotspot event, the deployed UAV must have enough on-board power to satisfy the downlink communication demand. In order to find a qualified UAV with sufficient energy, the network operator should estimate the required transmit power, based on the real-time cellular traffic load. These challenges, in turn, motivate the need for a comprehensive prediction of cellular traffic, and a predictive approach for UAV deployment [9]. To this end, machine learning (ML) techniques can be applied to analyze the traffic pattern, thus estimating the cellular traffic demand within the target system. Given the predicted traffic load, each BS can detect hotspot events and request suitable UAVs to alleviate network congestion.

Another practical challenge facing the deployment of on-demand aerial wireless service is to incentivize cooperation between the ground cellular network and the UAV operators. As shown in [10], UAV BSs and the ground cellular BSs can belong to different operators who seek to selfishly maximize their own, individual benefits. Hence, in order to request a UAV's assistance, a ground BS must offer an appropriate economic reward to the UAV operator for its aerial wireless service. However, given that the ground BS operator has no prior knowledge about each UAV,

there is no guarantee that the requested UAV is able to provide enough transmit power to satisfy the downlink data demand. Therefore, designing an effective incentive mechanism is necessary to ensure a truthful information exchange between the UAV and BS systems.

A. Related Works

The optimal deployment of UAVs as aerial BSs has recently attracted significant attention [11]–[13]. In [11], the authors studied the optimal locations and coverage areas of aerial BSs under the objective of minimizing the transmit power. The work in [12] derived the minimum number of UAVs to satisfy the coverage and capacity constraints of the wireless system. In [13], the authors jointly optimized the UAV trajectory and the network resource allocation in order to maximize the throughput to ground users. The problem of traffic offloading from an existing wireless network via UAV BSs has been addressed in [14]–[17]. In [14], the allocation problem of UAVs to each geographic area was investigated to improve the spectral efficiency and reduce the delay. In [15] and [16], the authors optimized the trajectory of UAVs to provide wireless services to the cell-edge users. In [17], an unsupervised learning approach was presented to solve the 3D deployment of a fleet of UAVs for traffic offloading. However, most of the existing works [11]–[17] assumed that the traffic demand of the cellular users is known a priori, which is challenging to estimate in a practical network. Furthermore, the works [11]–[17] optimized the performance of the cellular network in a centralized approach which assumes all UAVs belong to the same entity. Given the fact that the UAVs can belong to multiple operators, a new framework is needed to consider the individual utility of UAVs in the aerial communication service, while optimizing the performance of the ground cellular networks.

Meanwhile, in [18]–[20], a number of ML approaches are proposed to predict the data demands of cellular networks. In [18], a traffic prediction framework was proposed to model the cellular data in the temporal and spatial domains. In [19], the authors proposed an ML framework, based on pattern modeling, to predict the locations of mobile users during daily activities. The work [20] provided surveys that focused on the general use of ML algorithms in cellular networks. Furthermore, the prior art in [21]–[23] studied the use of ML techniques to improve the performance of UAV-aided communications. In [21], an ML framework based on liquid state machine is proposed to optimize the caching content of each UAV, as well as the resource allocation strategies. In [22], the authors investigated an ML approach to construct a radio map for autonomous path planning and positioning of UAVs. In [23], ML algorithms are applied to detect

and distinguish aerial users from the ground mobile users. However, most of the works in [18]–[23] aim to build an ML model to predict regular cellular traffic patterns, while hotspot and network congestion events are considered as an anomaly and excluded from these studies. In fact, none of the approaches proposed in [18]–[23] can effectively identify the hotspot areas or accurately predict excessive traffic load during the congestion events. Therefore, the results of these prior works cannot enable a predictive UAV deployment for on-demand cellular service to alleviate the traffic congestion.

B. Contributions

The main contribution of this paper is a novel framework for optimally deploying UAVs to assist a ground cellular network in alleviating its downlink traffic congestion during hotspot events. The proposed framework divides the deployment process into four, inter-related and sequential stages: learning stage, association stage, movement stage, and service stage. For each stage, we evaluate the performance of the proposed framework, using an open-source dataset in [24], and compare the economic revenues of the BS and UAV network operators with a baseline, event-driven allocation approach. Our main contributions include:

- A novel framework, based on the weighted expectation maximization (WEM) approach, is proposed to predict the downlink traffic demand for each cellular system in the learning stage. In particular, the proposed approach can identify the user distribution, predict the cellular data demand, and pinpoint the hotspot areas within the cellular system.
- In the association stage, in order to ensure that the employed UAV can satisfy the downlink demand, the framework of contract theory [25] is introduced for each overloaded BS to jointly design the transmit power and unit reward of the target UAV. We analytically derive the sufficient and necessary conditions needed to guarantee a truthful information exchange between the BS and UAV network operators. Once the association stage is done, each BS will have employed a proper UAV (with sufficient on-board energy) to assist its downlink cellular service.
- Simulation results show that the normalized root mean-square error (NRMSR) of the proposed ML approach is lower than 12%. Compared with a conventional expectation maximization (EM) approach, the proposed method yields a significant advantage to predict the traffic demand, as the downlink traffic load in the cellular system becomes spatially uneven. Furthermore, simulation results show that the designed contract can ensure a non-

negative payoff of each employed UAV. Meanwhile, each UAV will truthfully reveal its communication capability by accepting the contract designed for itself.

- We compare the performance of the proposed UAV deployment approach with an event-driven method, which deploys the closest UAV onto the hotspot area without traffic prediction and contract design. Our numerical results show that the proposed predictive method enables UAV operators to provide efficient downlink service for hotspot users, and significantly improves the economic revenues of both the BS and UAV network operators, compared with the event-driven approach.

The rest of this paper is organized as follows. In Section II, we present the system model. The problem formulation is given in Section III. In Section IV, the ML approach is proposed to predict downlink traffic demands. In Section V, the feasible contract is designed with the optimal UAV being employed to offload the cellular traffic. Simulation results are presented in Section VI. Finally, conclusions are drawn in Section VII.

II. SYSTEM MODEL

Consider a set \mathcal{I} of I cellular BSs providing downlink wireless service to a group of user equipments (UEs) in a geographical area \mathcal{A} . Each BS $i \in \mathcal{I}$ serves an area \mathcal{A}_i , such that $\cup_{i \in \mathcal{I}} \mathcal{A}_i = \mathcal{A}$, and $\mathcal{A}_i \cap \mathcal{A}_k = \emptyset$ for any $i, k \in \mathcal{I}$, $i \neq k$. A set \mathcal{J} of J flying UAVs can be used as aerial BSs that provide additional cellular service towards the UEs, if the hotspot events happen in the ground cellular network. We assume that the group BSs and UAVs belong to different network operators, and different frequency bands are used for the ground and aerial downlink transmissions, separately. At each UE, a single antenna is equipped, which can receive signals from both the ground BS and the flying UAV. Initially, a UE will connect to one of the ground BSs. However, as shown in Fig. 1, if a ground BS $i \in \mathcal{I}$ is overloaded in the downlink, BS i can request the assistant of a UAV to offload the service of some UEs. We assume that a UAV only serves the UEs of a single BS at each time, while each BS can employ multiple UAVs, based on the cellular traffic amount. In this regard, if the downlink traffic demand at the level of a given BS is excessive, such that no single UAV is capable to alleviate communication congestion, then the BS will divide the offloaded UEs into multiple spatially-disjoint sets, and request an individual UAV for each UE set, independently. In order to serve the downlink UEs more efficiently, each UAV is equipped with a directional antenna array that enables beamforming transmissions [26]. As a result, interference between different UAV networks is negligible.

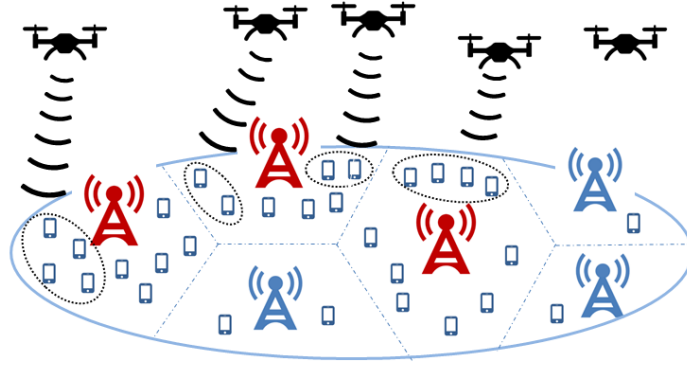


Fig. 1: The red BSs are having excessive traffic load in the downlink, thus each red BS requests a UAV to offload a part of UEs to the aerial cellular system.

A. Air-to-ground downlink communications

The path loss of the air-to-ground communication link from a typical UAV located at $\mathbf{x} \in \mathbb{R}^3$ to a typical ground UE that is located at $\mathbf{y} \in \mathbb{R}^3$ can be given by [27]:

$$h[\text{dB}](\mathbf{x}, \mathbf{y}) = 20 \log \left(\frac{4\pi f_c \|\mathbf{x} - \mathbf{y}\|}{c} \right) + \xi(\mathbf{x}, \mathbf{y}), \quad (1)$$

where f_c is the carrier frequency of UAV downlink communications, $\|\mathbf{x} - \mathbf{y}\|$ is the UAV-UE distance, c is the speed of light, and $\xi(\mathbf{x}, \mathbf{y})$ is the additional path loss of the air-to-ground channel, compared with the free space propagation. The value of $\xi(\mathbf{x}, \mathbf{y})$ can be modeled as a Gaussian distribution with different parameters $(\mu_{\text{LOS}}, \sigma_{\text{LOS}}^2)$ and $(\mu_{\text{NLOS}}, \sigma_{\text{NLOS}}^2)$ for the LOS and non-line-of-sight (NLOS) links, respectively. Then, the achievable data rate from a UAV $j \in \mathcal{J}$ located at \mathbf{x}_j to a UE located at $\mathbf{y} \in \mathcal{A}_i$ is

$$r_{ij}(\mathbf{x}_j, \mathbf{y}, p_j) = w \log_2 \left(1 + \frac{g(\mathbf{x}_j, \mathbf{y}) p_j}{h(\mathbf{x}_j, \mathbf{y}) w n_0} \right), \quad (2)$$

where w is the downlink bandwidth of each UAV, $g(\mathbf{x}_j, \mathbf{y})$ is the antenna gain of UAV j towards the UE located at \mathbf{y} , p_j is the transmit power of UAV j , $h(\mathbf{x}_j, \mathbf{y})$ is the path loss in linear scale, and n_0 is the average noise power spectrum density at the UE. The probability of having a LOS link between UAV j located at \mathbf{x}_j and the UE located at \mathbf{y} is given by [28]:

$$P_{\text{LOS}}(\mathbf{x}_j, \mathbf{y}) = \frac{1}{1 + a \exp(-b[\frac{180}{\pi} \varphi(\mathbf{x}_j, \mathbf{y}) - a])}, \quad (3)$$

where a and b are constant values that depend on the communication environment (rural, urban, etc.), $\varphi(\mathbf{x}_j, \mathbf{y}) = \sin^{-1}(\frac{H_j}{\|\mathbf{x}_j - \mathbf{y}\|})$ is the elevation angle, and H_j is the altitude of UAV j . Then, the NLOS probability is $P_{\text{NLOS}}(\mathbf{x}_j, \mathbf{y}) = 1 - P_{\text{LOS}}(\mathbf{x}_j, \mathbf{y})$. Consequently, the average downlink rate between a UAV j and a UE at $\mathbf{y} \in \mathcal{A}_i$ will be:

$$\bar{r}_{ij}(\mathbf{x}_j, \mathbf{y}, p_j) = P_{\text{LOS}}(\mathbf{x}_j, \mathbf{y}) r_{ij}^{\text{LOS}}(\mathbf{x}_j, \mathbf{y}, p_j) + P_{\text{NLOS}}(\mathbf{x}_j, \mathbf{y}) r_{ij}^{\text{NLOS}}(\mathbf{x}_j, \mathbf{y}, p_j). \quad (4)$$

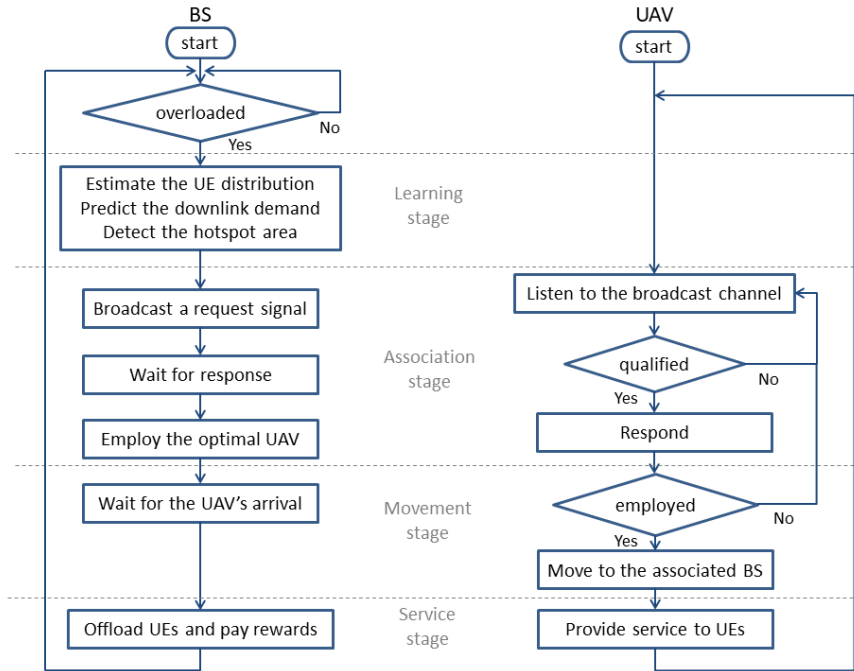


Fig. 2: Flowchart of the proposed UAV predictive deployment process for each BS (left) and each UAV (right).

In order to serve multiple downlink UEs, each UAV applies a time-division-multiple-access (TDMA) technique¹ that divides the time resource evenly among all served UEs, and all bandwidth will be allocated to one single UE during each time slot [29]. By using suitable uplink control signals, the UAV-UE channel can be accurately measured, and thus, the beamforming of UAV's antennas can be properly optimized towards the served UE. Consequently, the average capacity that UAV j can provide to the group of UEs from BS i will be

$$C_{ij}(\mathbf{x}_j, p_j) = \int_{\mathcal{A}_i^c} \bar{r}_{ij}(\mathbf{x}_j, \mathbf{y}, p_j) f_i(\mathbf{y}) d\mathbf{y}, \quad (5)$$

where $\mathcal{A}_i^c \subset \mathcal{A}_i$ is the hotspot area, and $f_i(\mathbf{y})$ is the spatial distribution of UEs with $\int_{\mathcal{A}_i^c} f_i(\mathbf{y}) d\mathbf{y} = 1$. In other words, when downlink congestion happens, BS i detects the congested area \mathcal{A}_i^c and offloads the UEs within \mathcal{A}_i^c to the target UAV.

B. UAV deployment process

Given the average downlink capacity of each UAV in (5), the next step is to deploy suitable UAVs to offload the traffic of a given overloaded BS and, hence, alleviate the downlink congestion of the ground cellular network. To facilitate the analysis, we assume that each UAV serves the

¹The focus of this work is on the deployment stage and, hence, we do not optimize the multiple access scheme type or operation. Optimizing multiple access can be done post-deployment and will be subject to future work.

associated BS for a constant time interval T . As shown in Fig. 2, this deployment process can be divided into four sequential stages: learning stage, association stage, movement stage, and service stage. The details of each stage are given as next:

1) *Learning stage*: For each BS $i \in \mathcal{I}$, once the downlink communication exceeds its network capacity, a learning stage with a fixed duration τ starts. During τ , BS i collects the downlink transmission record $\mathcal{S}_i = \{(s, \mathbf{y}, t) | \mathbf{y} \in \mathcal{A}_i, t \in [\Delta t, 2\Delta t, \dots, \tau]\}$, where s is the downlink data rate that BS i provides to the UE located at \mathbf{y} at time t , and Δt is the time slot during which the downlink rate can be considered to be constant. Since BS i does not know the hotspot area \mathcal{A}_i^c and the UE distribution $f_i(\mathbf{y})$ when congestion occurs, a learning stage is necessary to estimate the spatial distribution of UEs and the traffic demand of the on-going hotspot event.

Considering common events, such as sport games and outdoor concerts, where mobile users are often confined to seated or geographically constrained spaces in which mobility is either scarce or very low. Therefore, we assume that the UE distribution $f_i(\mathbf{y})$ during one T is time-invariant. Furthermore, to estimate the traffic demand within the congested area, a spatial function $S_i(\mathbf{y})$ is used to evaluate the average data rate required by UEs at each location $\mathbf{y} \in \mathcal{A}_i$. Consequently, the total data demand d_i from a hotspot area \mathcal{A}_i^c during a time interval T will be given by:

$$d_i = \int_t^{t+T} \int_{\mathbf{y} \in \mathcal{A}_i^c} S_i(\mathbf{y}) d\mathbf{y} dt = T \int_{\mathbf{y} \in \mathcal{A}_i^c} S_i(\mathbf{y}) d\mathbf{y}. \quad (6)$$

The proposed approach for estimating the UE distribution and traffic demand will be discussed in Section IV.

The last step of the learning stage is for BS i to estimate whether one UAV is sufficient to alleviate its downlink congestion, and to calculate the optimal location of each target UAV. Following from [11], given the UE distribution $f_i(\mathbf{y})$ and the hotspot area \mathcal{A}_i^c , the location \mathbf{x}_{ij}^* of a target UAV j in serving BS i can be derived in a way to minimize the transmit power $p_{ij}(\mathbf{x}_{ij}^*, \rho_i^c)$, while satisfying the average rate requirement ρ_i^c per UE. The average rate is defined by $\rho_i^c = \frac{d_i}{TQ_i^c} = \frac{\int_{\mathbf{y} \in \mathcal{A}_i^c} S_i(\mathbf{y}) d\mathbf{y}}{Q_i^c}$, where Q_i^c is the number of UEs within \mathcal{A}_i^c . Therefore, the optimal service location of the target UAV can be calculated by BS i , prior to the UAV's deployment. We define p_{\max} to be the maximum transmit power of each UAV, which is limited by the antennas' hardware. Note that, once $d_i > TC_{ij}(\mathbf{x}_{ij}^*, p_{\max})$, any UAV $j \in \mathcal{J}$ will no longer be sufficient to satisfy the downlink demand d_i . In this case, BS i will divide the offloaded UEs into N disjoint subsets, where N is the minimal integer needed to guarantee that, for each subset $n = 1, \dots, N$,

$$d_i(n) < TC_{ij}(\mathbf{x}_{ij}^*(n), p_{\max}). \quad (7)$$

Next, each UE set will be associated with a UAV, independently.

2) *Association stage* : In the association stage, each overloaded BS i requests the assistance of a UAV, by broadcasting a signal with the downlink demand $d_i(n)$ and the service location $\mathbf{x}_{ij}^*(n)$ for each UE subset. A first-call-first-serve scheme is applied, and each BS $i \in \mathcal{I}$ will listen to the broadcast channel before sending the signal. If the channel is occupied by another BS, then BS i will wait until the on-going association is completed. For each BS i , the goal is to request a UAV that has enough on-board power to meet the downlink demand d_i of UEs within \mathcal{A}_i^c . The optimal UAV association to each overloaded BS will be studied in Section V.

3) *Movement stage*: After the association stage, the selected UAV j starts to move from its current location \mathbf{x}_j to the service point \mathbf{x}_{ij}^* of its target BS i . The duration t_{ij} of the movement stage depends on the distance $\|\mathbf{x}_j - \mathbf{x}_{ij}^*\|$ and the average speed v_j of UAV j .

4) *Service stage*: Once it reaches the service point, UAV j will provide downlink communications to its group of associated UEs for a time period $T - t_{ij}$. Note that, during the movement and service stages, the employed UAV is fully dedicated to its associated BS. Thus, the UAV cannot be requested by any other BSs until the end of its current service. Furthermore, to guarantee a sufficient service time, we must have: $t_{ij} \leq \frac{T}{2}$. Otherwise, UAV j is not a potential choice for BS i .

Here, in order to optimally associate a UAV to each overloaded ground BS, we first define a utility function that each BS aims to maximize when selecting a UAV to offload cellular traffic in Section II-C. Meanwhile, the UAV's utility function is given in Section II-D that defines an economic payoff of each UAV from serving an overloaded BS.

C. Utility function of a ground BS

In the considered network, by using TDMA, the employed UAV j will evenly divide the service time $T - t_{ij}$ to all downlink UEs within \mathcal{A}_i^c . Considering the signal overhead and channel measurement process, we assume the total efficient transmission time is $\eta(T - t_{ij})$, where $\eta \in (0, 1)$. Therefore, based on the average downlink capacity in (5), the achievable data amount that UAV j can provide to the UEs of BS i is

$$B_{ij}(p_j) = \eta(T - t_{ij})C_{ij}(p_j). \quad (8)$$

Note that, the movement duration t_{ij} and the transmit power p_j are private information for UAV j , and, thus, BS i cannot know their values during the service request process. Then, the utility of BS i , by employing UAV j to offload the excess cellular traffic, will be:

$$U_{ij}(u_i, p_j, d_i) = \beta B_{ij}(p_j) - u_i d_i, \quad (9)$$

where β is the payment from each UE to BS i (per bit of downlink data service), and u_i is the unit payment that BS i gives to UAV j (per bit of aerial data transmission). Thus, the first term in (9) represents the reward that BS i gets from its UEs by employing UAV j to provide aerial cellular service, and the second term is the total payment that BS i gives to UAV j , based on the estimated downlink demand d_i .

D. Energy model and utility function of a UAV

In the considered problem, the power consumption of each UAV consists of three main components: the aforementioned transmit power p_j , the propulsion power m , and the hovering power p_h . For tractability and as done in [30], we ignore the acceleration and deceleration stages during the UAV's movement, and consider the propulsion power m to be constant, given an average flying speed. Then, the travel time t_{ij} can be uniquely determined based on the moving distance $\|\mathbf{x}_j - \mathbf{x}_{ij}^*\|$ [31]. For each UAV j , let E_j be its available on-board energy before the movement stage. Then, during the service stage, the maximum available power that UAV j can use for downlink transmissions will be $p_{ij}^{\max} = \frac{E_j - mt_{ij} - p_h(T - t_{ij})}{T - t_{ij}}$, where mt_{ij} is the energy consumed during the UAV's movement, and $p_h(T - t_{ij})$ is the hovering energy during the service stage. Therefore, the transmit power p_j will fall within $[p_{ij}(\mathbf{x}_{ij}^*, \rho_i^c), \min\{p_{ij}^{\max}, p_{\max}\}]$, where $p_{ij}(\mathbf{x}_{ij}^*, \rho_i^c)$ is the minimum required power to satisfy the downlink data demand, and p_{\max} is the maximum transmit power. Without loss of generality, we assume that $p_{ij}(\mathbf{x}_{ij}^*, \rho_i^c) \leq \min\{p_{ij}^{\max}, p_{\max}\}$ holds. Otherwise, UAV j is not a potential option for BS i . Consequently, the utility that a UAV $j \in \mathcal{J}$ can achieve from providing the aerial cellular service to the UEs of BS i is

$$R_{ij}(u_i, p_j, d_i) = u_i d_i - \alpha [p_j(T - t_{ij}) + mt_{ij}], \quad (10)$$

where α is a unit cost per Joule of UAV's on-board energy. The first term in (10) is the reward that UAV j obtains from serving BS i , and the second term in (10) is the energy cost, where $p_j(T - t_{ij})$ is the total transmit energy. Here, we assume that if a UAV is not associated to any

BS, it will hover in the air to listen to the broadcast channel. Therefore, the hovering power p_h is inevitable and, without loss of generality, we exclude p_h from the UAV's cost function².

Note that, the data demand d_i is estimated by BS i during the learning stage. Therefore, during the association stage, d_i in (9) and (10) is considered as a constant. The unit payment u_i and the transmit power p_j are the variables, controlled by BS i and UAV j , respectively.

III. PROBLEM FORMULATION

The objective of a BS in face of downlink congestion is to employ a suitable UAV with enough on-board power to offload excessive downlink traffic, while maximizing the utility function in (9). Meanwhile, the goal of each UAV is to serve an overloaded BS, such that its utility in (10) can be optimized. However, by comparing (9) and (10), we realize that $\arg \max_{u_i, p_j} U_{ij} = \arg \min_{u_i, p_j} R_{ij}$ and $\arg \max_{u_i, p_j} R_{ij} = \arg \min_{u_i, p_j} U_{ij}$. Therefore, each BS-UAV pair has conflicting interests. Given that the ground BSs and UAVs belong to different operators, each will maximize its individual utility. The conflict between each BS and each UAV is irreconcilable.

Moreover, we note that the values of the unit payment u_i and the data demand d_i will be broadcast by BS i during the association stage. Thus, each UAV j has all necessary information to determine its utility. However, since the transmit power p_j is the private information of UAV j that BS i does not know, the utility of the requesting BS is always undetermined. Therefore, BS i has a motivation to jointly design the value of (u_i, p_j) , so as to guarantee that the employed UAV j will truthfully provide enough power to serve the downlink UEs. In particular, an incentive mechanism is necessary to ensure that the values of (u_i, p_j) are beneficial for both the BS and UAV operators, and the interest conflict between the group UAVs and BSs can be properly resolved. Therefore, we let $\phi_{ij} = (u_i, p_j)$ be a *traffic offload contract*, which defines the values of p_j and u_i if BS i employs UAV j to offload UEs. In order to understand the relationship between the unit payment u_i and the transmit power p_j , we divide both sides of (10) by $\alpha(T - t_{ij})$ and rewrite the utility of UAV j as follows:

$$\begin{aligned} \tilde{R}_{ij}(u_i, p_j, d_i) &= \frac{d_i}{\alpha(T - t_{ij})} u_i - p_j - \frac{m t_{ij}}{T - t_{ij}}, \\ &= \theta_{ij} u_i - p_j - M_{ij}, \end{aligned} \tag{11}$$

²To include the hovering power, one can add the constant value of p_h onto p_j , which will not change the subsequent analysis.

where the values of $\theta_{ij} = \frac{d_i}{\alpha(T-t_{ij})}$ and $M_{ij} = \frac{mt_{ij}}{T-t_{ij}}$ are determined for each BS-UAV pair.

Since θ_{ij} determines the sensitivity of \tilde{R}_{ij} to the increase of u_i and p_j in (11), its value is essential for the joint design of (u_i, p_j) . Therefore, we define θ_{ij} as the *type* of UAV j with respect to BS i , and the range of θ_{ij} is denoted by $\Theta = [\theta^{\min}, \theta^{\max}]$, with $\theta^{\min} > 0$. However, due to the privacy of t_{ij} , the type θ_{ij} of each UAV $j \in \mathcal{J}$ is unknown for BS i . In order to design the contract without knowing each UAV's type, before broadcasting the request signal, BS i will design a set of contracts $\Phi_i(\Theta) = \{\phi_{ij}(\theta_{ij}) | \forall \theta_{ij}\} = \{(u_i(\theta_{ij}), p_j(\theta_{ij})) | \forall \theta_{ij}\}$ for all UAV types $\theta_{ij} \in \Theta$, where $u_i(\theta_{ij})$ represents the payment that BS i pays to UAV j per bit of data, given that UAV j is of type θ_{ij} , and $p_j(\theta_{ij})$ is the transmit power that UAV j of type θ_{ij} provides to serve BS i . Then, (11) becomes $\tilde{R}(\theta_{ij}) = \theta_{ij}u_i(\theta_{ij}) - p_j(\theta_{ij}) - M_{ij}$.

Meanwhile, to ensure that the employed UAV will accept the contract of its own type and provide enough transmit power to meet the downlink demand, two constraints, based on contract theory [25], must be considered, which are individual rationality (IR) condition and incentive compatibility (IC) condition, defined as follows.

Definition 1 (Individual Rationality). *A contract designed by BS i satisfies the IR constraint, if a UAV of any type $\theta_{ij} \in \Theta$ will receive a non-negative payoff from BS i by accepting the contract item for type θ_{ij} , i.e. $\theta_{ij}u_i(\theta_{ij}) - p_j(\theta_{ij}) - M_{ij} \geq 0, \forall \theta_{ij} \in \Theta$.*

A contract satisfying the IR condition guarantees that the reward that each UAV $j \in \mathcal{J}$ can obtain from serving BS i is great than or equal to zero. Compared with the non-employed state in which the payoff is always zero, each UAV is willing to accept the contract from the requesting BS, as long as its contract satisfies the IR condition.

Definition 2 (Incentive Compatibility). *A contract designed by BS i satisfies the IC constraint, if a UAV of type θ_{ij} will get the highest utility from BS i by accepting the contract designed for its own type θ_{ij} , compared with all the other types θ in Θ , i.e. $\theta_{ij}u_i(\theta_{ij}) - p_j(\theta_{ij}) - M_{ij} \geq \theta_{ij}u_i(\theta) - p_j(\theta) - M_{ij}, \forall \theta \in \Theta$.*

A contract satisfying IC condition guarantees that each UAV j will only accept the contract designed for its own type θ_{ij} , since accepting the contract of any other type $\theta \in \Theta$ will result in a lower or the same reward. A contract satisfying both IR and IC conditions is called a *feasible* contract, which ensures the UAV will accept and only accept the contract designed for its type.

Consequently, for each BS $i \in \mathcal{I}$ in face of downlink traffic congestion, the objective is to

maximize its utility in (9), by estimating the downlink data demand d_i within the hotspot area \mathcal{A}_i^c , designing the contract set Φ_i for each UAV of any type in Θ , and determining an optimal UAV $j \in \mathcal{J}$ to offload the excessive cellular service. We formulate this predictive UAV deployment problem as follows,

$$\max_{\{(u_i(\theta_{ij}), p_j(\theta_{ij})) | \forall \theta_{ij}, j \in \mathcal{J}\}} U_{ij}(u_i(\theta_{ij}), p_j(\theta_{ij}), d_i), \quad (12a)$$

$$\text{s. t. } R_{ij}(\theta_{ij}) \geq 0, \quad (12b)$$

$$R_{ij}(\theta_{ij}) \geq R_{ij}(\theta), \forall \theta \in \Theta, \quad (12c)$$

$$p_{ij}(\mathbf{x}_{ij}^*, \rho_i^c) \leq p_j(\theta_{ij}) \leq \min\{p_{ij}^{\max}, p_{\max}\}, \quad (12d)$$

$$t_{ij} \leq T/2, \quad (12e)$$

$$d_i > 0, u_i(\theta_{ij}) > 0. \quad (12f)$$

The objective function (12a) is the utility that BS i obtains from employing UAV j of type θ_{ij} . (12b) and (12c) are the IR and IC constraints, respectively. (12d) is the constraint on the transmit power, and (12e) limits the maximum travel time. (12f) imposes a positive downlink demand within \mathcal{A}_i^c , and a positive unit payment.

Note that, the IC constraint (12c) is an optimization problem, which must be first addressed in order to guarantee that each UAV receives the highest payoff by accepting the contract item of its own type. Meanwhile, given any $\theta_{ij} \in \Theta$, the objective function and all constraints in (12) are jointly determined. Thus, the variable θ_{ij} becomes the key to finding the optimal association result. In order to simplify the optimization problem (12), we can derive the necessary and sufficient conditions for IC and IR constraints, based on the UAV type θ_{ij} , which essentially reduces to the problem of designing a feasible contract.

Consequently, in order to solve the predictive UAV deployment problem in (12), first, a learning-based approach is proposed for each BS $i \in \mathcal{I}$ to predict the downlink demand d_i of the offloaded UEs in Section IV. Next, the feasible traffic offload contract Φ_i is developed in Section V, with the optimal UAV being selected to maximize the utility of the requesting BS i .

IV. LEARNING STAGE: ESTIMATION OF CELLULAR TRAFFIC DEMAND

In this section, our goal is to estimate the UE distribution and the downlink data demand during the hotspot event of a BS. This estimation is necessary to solve (12) because the downlink data demand d_i is considered as a known value in the association stage, which determines the type

θ_{ij} of each UAV j with respect to the overloaded BS i . To enable an accurate modeling, each BS i collects the downlink transmission records \mathcal{S}_i during the learning stage. For notational simplicity, let N be the total number of records in \mathcal{S}_i . Then, the downlink transmission dataset \mathcal{S}_i can be rewritten as $\{(s_n, \mathbf{y}_n, t_n) | n = 1, \dots, N\}$. Given the aggregated locations of the UEs within the hotspot area, the user distribution and the downlink traffic demand are assumed to be time-invariant during T . Based on \mathcal{S}_i , we extract the spatial distribution $f_i(\mathbf{y})$ of the downlink UEs in Section IV-A, and, then, we model the downlink data rate $S_i(\mathbf{y})$ and determine the hotspot area \mathcal{A}_i^c in Section IV-B. Once this is done, the average capacity of each UAV can be given by (5), and the downlink data demand d_i will be found from (6).

A. Estimation of the UE distribution

Given the downlink transmission record \mathcal{S}_i , BS i can model the UE distribution, using the location information $\mathcal{Y} = \{\mathbf{y}_1, \dots, \mathbf{y}_N\}$, where each data point $\mathbf{y}_n \in \mathcal{Y}$ indicates the existence of a downlink UE. We assume that the UEs' locations follow a latent distribution $f_i(\mathbf{y})$, and each record \mathbf{y}_n is an independent sample from this distribution. A Gaussian mixture model (GMM), which is the weighted sum of multiple Gaussian distributions, can model the distribution of downlink UEs, as follows:

$$f_i(\mathbf{y}) = \sum_{l=1}^L \omega_l \mathcal{N}(\mathbf{y} | \boldsymbol{\mu}_l, \boldsymbol{\Sigma}_l), \quad (13)$$

where L is the number of Gaussian distributions, $\omega_l \in (0, 1)$ is the weight of the l -th Gaussian with $\sum_l \omega_l = 1$, and $\boldsymbol{\mu}_l, \boldsymbol{\Sigma}_l$ are the mean and the variance of the l -th Gaussian. The value of ω_l represents the probability that the data point \mathbf{y} is generated by the l -th distribution. GMM has been widely applied in [32]–[34] to model the distribution of a latent variable based the sampled data. In particular, due to its special feature of multiple clusters, GMM is a appropriate model of the UE distribution in the congested cellular network, where each hotspot area with a excessive UE density corresponds to a Gaussian center in the GMM.

Given the sampled location record \mathcal{Y} , the expectation-maximization (EM) algorithm [34] can be applied to optimize the parameters $\{\omega_l, \boldsymbol{\mu}_l, \boldsymbol{\Sigma}_l\}_{l=1, \dots, L}$ in (13) via an iterative approach, which maximizes the following log of the likelihood function:

$$\ln p(\mathcal{Y} | \boldsymbol{\omega}, \boldsymbol{\mu}, \boldsymbol{\Sigma}) = \ln \prod_{n=1}^N \left(\sum_{l=1}^L \omega_l \mathcal{N}(\mathbf{y}_n | \boldsymbol{\mu}_l, \boldsymbol{\Sigma}_l) \right). \quad (14)$$

After initialization, the EM algorithm alternates between the E and M steps. In the E step, the posterior probability that \mathbf{y}_n is generated by the l -th Gaussian is calculated by

$$v_{nl} = \frac{\omega_l \mathcal{N}(\mathbf{y}_n | \boldsymbol{\mu}_l, \boldsymbol{\Sigma}_l)}{\sum_{z=1}^L \omega_z \mathcal{N}(\mathbf{y}_n | \boldsymbol{\mu}_z, \boldsymbol{\Sigma}_z)}. \quad (15)$$

Then, in the M step, the parameters are updated using the posterior probability (15) by

$$\boldsymbol{\mu}_l = \frac{\sum_n v_{nl} \mathbf{y}_n}{\sum_n v_{nl}}, \quad \boldsymbol{\Sigma}_l = \frac{\sum_n v_{nl} (\mathbf{y}_n - \boldsymbol{\mu}_l)(\mathbf{y}_n - \boldsymbol{\mu}_l)^T}{\sum_n v_{nl}}, \quad \omega_l = \frac{\sum_n v_{nl}}{N}. \quad (16)$$

After each EM iteration, the updated parameters will result in an increase of the log likelihood function in (14), and the algorithm is guaranteed to converge to a local optimum [34]. Moreover, the mixture number L in the GMM needs to be optimized over an integer set $\{L^{\min}, \dots, L^{\max}\}$, using the validation data. The purpose of optimizing the mixture number L is to guarantee the trained model is accurate, as well as general enough, to represent the latent distribution of UEs' locations. Therefore, BS i needs to train multiple models with different mixture numbers, and chooses the optimal value of L from $\{L^{\min}, \dots, L^{\max}\}$ that maximizes the likelihood function.

B. Estimation of the downlink data rate

In order to predict the downlink demand d_i , the spatial feature of the cellular traffic needs to be properly captured by each overloaded BS i , based on the real-time transmission record \mathcal{S}_i . Given the assumption that the data demand is time-invariant during T , the temporal variance in \mathcal{S}_i can be eliminated by averaging the downlink rate at each location over the learning duration τ . Thus, we define the *density* of the downlink data rate at location $\mathbf{y} \in \mathcal{A}_i$ as

$$\bar{S}_i(\mathbf{y}) = \frac{\sum_{(s_n, \mathbf{y}, t_n) \in \mathcal{S}_i} s_n \Delta t}{\tau}, \quad (17)$$

which is the average rate from BS i towards UEs located at \mathbf{y} during the learning stage. To generalize the traffic density $\bar{S}_i(\mathbf{y})$ into a continuous model that captures the spatial features of the UEs' downlink demand, a Gaussian mixture function (GMF) is proposed as follow,

$$S_i(\mathbf{y}) = \sum_{k=1}^K \pi_k \exp\left(\frac{-(\mathbf{y} - \boldsymbol{\mu}_k)^T \boldsymbol{\Sigma}_k^{-1} (\mathbf{y} - \boldsymbol{\mu}_k)}{2}\right), \quad (18)$$

where K is the number of basis functions, $\pi_k > 0$ is the linear coefficient, and $\boldsymbol{\mu}_k \in \mathcal{A}_i$ and $\boldsymbol{\Sigma}_k$ are the mean and variance of the k -th Gaussian function in the GMF. Therefore, the traffic density at location \mathbf{y} is modeled by the sum of K Gaussian functions with coefficient $\{\pi_k\}_{k=1, \dots, K}$.

However, it should be noted that GMF in (18) is different from GMM in (13) for two reasons. First, a GMF does not have a probabilistic interpretation. In particular, (18) is a deterministic

function with respect to \mathbf{y} , which calculates the traffic density at location \mathbf{y} , by adding the values of K Gaussian function with different linear coefficients. Second, different from the weight in GMM where $\omega_l \in (0, 1)$ and $\sum_l \omega_l = 1$, the value of each linear coefficient π_k is usually greater than one, and no constraint exists on their sum. On the other hand, although (18) has a similar expression to the traditional linear regression (LR) model, a significant difference between GMF and LR is that the parameters π_k , $\boldsymbol{\mu}_k$ and $\boldsymbol{\Sigma}_k$ of each Gaussian function in (18) are undetermined. Therefore, the existing algorithm for the linear regression with fixed basis functions is not applicable in this problem.

In order to properly model the downlink traffic density \bar{S}_i , the parameters $\{\pi_k, \boldsymbol{\mu}_k, \boldsymbol{\Sigma}_k\}_{k=1, \dots, K}$ in (18) need to be optimized. Since the function value $S_i(\mathbf{y})$ is the density of the downlink data rate within a small neighborhood near \mathbf{y} , the weight π_k for each k in S_i is usually greater than one. Therefore, the EM method is not suitable to the traffic density modeling. Moreover, given that each data point \mathbf{y}_n has a different traffic density $\bar{S}_i(\mathbf{y}_n)$, the weight of each location \mathbf{y}_n in determining the parameter values should vary accordingly. Therefore, by adding the weight $\bar{S}_i(\mathbf{y}_n)$ to each data point \mathbf{y}_n , a weighted expectation maximization (WEM) algorithm [1] is proposed to find the parameters of the traffic density model $S_i(\mathbf{y})$ in (18).

In WEM method, the initial value of each Gaussian center $\boldsymbol{\mu}_k$ is the location \mathbf{y}_k that has the k -th highest traffic density in $\bar{S}_i(\mathbf{y})$, where $\mathbf{y} \in \{\mathbf{y}_1, \dots, \mathbf{y}_N\}$. The initial variance $\boldsymbol{\Sigma}_k$ equals the identity matrix, and the weight $\pi_k = \frac{1}{K} \sum_{\mathbf{y}} \bar{S}_i(\mathbf{y})$. Then, the WEM algorithm updates the values of $\{\pi_k, \boldsymbol{\mu}_k, \boldsymbol{\Sigma}_k\}_{k=1, \dots, K}$ via an iterative approach. In the E step, the percentage that each Gaussian function k contributes to the value of the traffic density at location \mathbf{y}_n is evaluated via $v_{nk} = \frac{\pi_k \mathcal{N}(\mathbf{y}_n | \boldsymbol{\mu}_k, \boldsymbol{\Sigma}_k)}{\sum_{k=1}^K \pi_k \mathcal{N}(\mathbf{y}_n | \boldsymbol{\mu}_k, \boldsymbol{\Sigma}_k)}$, which is the same as the traditional EM method in (15). However, in the M step of WEM method, the parameters of each Gaussian function will be updated in a weighted approach, where the mean $\boldsymbol{\mu}_k$ is recalculated via

$$\boldsymbol{\mu}_k = \frac{\sum_n v_{nk} \mathbf{y}_n \bar{S}_i(\mathbf{y}_n)}{\sum_n v_{nk} \bar{S}_i(\mathbf{y}_n)}, \quad (19)$$

which is a weighted sum of all locations $\mathbf{y}_n \in \mathcal{Y}$, with both the posterior probability v_{nk} and the traffic density $\bar{S}_i(\mathbf{y}_n)$ being the weight of each location. Therefore, the location \mathbf{y}_n with a higher traffic density $\bar{S}_i(\mathbf{y}_n)$ will have a higher weight in determining the value of $\boldsymbol{\mu}_k$, and the center of Gaussian k will gradually be driven closer to the high-density locations. Similarly, the variance $\boldsymbol{\Sigma}_k$ and the linear coefficient π_k of each Gaussian function is also updated, with weights

$\bar{S}_i(\mathbf{y}_n)$, by

$$\Sigma_k = \frac{\sum_n v_{nk}(\mathbf{y}_n - \boldsymbol{\mu}_k)(\mathbf{y}_n - \boldsymbol{\mu}_k)^T \bar{S}_i(\mathbf{y}_n)}{\sum_n v_{nk} \bar{S}_i(\mathbf{y}_n)}, \quad \pi_k = \frac{\sum_n v_{nk} \bar{S}_i(\mathbf{y}_n)}{\sum_k \sum_n v_{nk} \bar{S}_i(\mathbf{y}_n)}. \quad (20)$$

Furthermore, similar to the EM approach, a WEM method will converge to a local optimum, which maximizes the weighted conditional log-likelihood function [1], and the number K of Gaussian functions needs to be optimized using a validation dataset.

The hotspot area \mathcal{A}_i^c is an area in which the traffic density is much higher compared with other locations in \mathcal{A}_i . Given the traffic density model S_i , we calculate the average traffic density in \mathcal{A}_i by $\bar{s}_i = \frac{1}{|\mathcal{A}_i|} \int_{\mathbf{y} \in \mathcal{A}_i} S_i(\mathbf{y}) d\mathbf{y}$, where $|\mathcal{A}_i|$ denotes the area of \mathcal{A}_i . Then, the potential hotspot areas are selected to be the neighborhoods $\mathcal{C}(\boldsymbol{\mu}_k)$ near the center $\{\boldsymbol{\mu}_k\}_{k=1, \dots, K}$ of each Gaussian component. Next, by calculating the traffic density in each $\mathcal{C}(\boldsymbol{\mu}_k)$, the mean $\boldsymbol{\mu}_k^*$ with the highest traffic density is chosen to be the hotspot center, and its neighborhood area, where the traffic density is higher than \bar{s}_i forms the hotspot area \mathcal{A}_i^c . The downlink UEs within \mathcal{A}_i^c will be offloaded to the aerial cellular network. If there exist multiple Gaussian centers with excessive cellular traffic, then each hotspot area will be associated with an individual UAV. Based on the traffic density model $S_i(\mathbf{y})$ and the hotspot area \mathcal{A}_i^c , the predicted data amount d_i for a time interval T can be calculated based on (6).

Given the downlink traffic demand d_i and the UE distribution $f_i(\mathbf{y})$, all variables in (12) have determined values, except for the unit payment u_i and the transmit power p_j . The next step to solve (12) is to jointly decide the value of (u_i, p_j) , by designing the feasible contract between an overloaded BS i with each UAV $j \in \mathcal{J}$.

V. ASSOCIATION STAGE: CONTRACT DESIGN AND UAV ALLOCATION

A. Contract design

Given the predicted traffic demand d_i , a BS $i \in \mathcal{I}$ can request a UAV and offload the UEs within the hotspot area \mathcal{A}_i^c , so that the future downlink congestion can be alleviated. However, to employ a qualified UAV to meet the downlink demand, each BS needs to carefully design the contract $\Phi_i = \{(u_i(\theta_{ij}), p_j(\theta_{ij})) | \forall \theta_{ij} \in \Theta\}$ for UAVs of any type θ_{ij} . The feasible contract satisfying the IR and IC conditions can motivate the truthful downlink service of the aerial network, such that each UAV $j \in \mathcal{J}$ will accept the contract designed for its own type and provide the required transmit power to serve the downlink UEs. Thus, to develop a feasible

contract set for the requesting BS, we first analyze the sufficient and necessary conditions for a contract to satisfy IC and IR constraints.

Proposition 1. *[Necessary Condition] For any $\theta_{ij}, \theta'_{ij} \in \Theta$, if $\theta_{ij} > \theta'_{ij}$, then $u_i(\theta_{ij}) \geq u_i(\theta'_{ij})$ and $p_j(\theta_{ij}) \geq p_j(\theta'_{ij})$.*

Proof. See Appendix A. □

Proposition 1 shows that for a typical UAV j in \mathcal{J} , if its type with respect to a typical BS i increases from θ'_{ij} to θ_{ij} , then it will receive a higher unit payment $u_i(\theta_{ij}) \geq u_i(\theta'_{ij})$ from BS i , and in return, it should provide a larger transmit power $p_j(\theta_{ij}) \geq p_j(\theta'_{ij})$ in its downlink transmission. Given the definition of $\theta_{ij} = \frac{d_i}{\alpha(T-t_{ij})}$, a higher type θ_{ij} indicates either a higher downlink demand d_i , or a longer travel time t_{ij} . In the first case, if the downlink demand d_i is higher, the employed UAV j must increase the transmit power to satisfy the larger communication needs. Therefore, $p_j(\theta_{ij})$ will increase. On the other hand, if UAV j travel for a long time t_{ij} to arrive the service area of BS i , then more mobility energy is consumed during the movement. In consequence, the unit payment $u_i(\theta_{ij})$ should be increased accordingly, to compensate for the longer travel. Therefore, a UAV of a higher type is required to provide more available transmit power, and will be given a higher unit payment. The conclusion in Proposition 1 will lead to the necessary and sufficient conditions of a feasible contract, as shown next.

Theorem 1. *[Necessary and Sufficient Condition] For a contract set $\Phi_i = \{(u_i(\theta_{ij}), p_j(\theta_{ij})) | \forall \theta_{ij}\}$, it is feasible if and only if all the following three conditions hold: (a) $\frac{dp_j(\theta_{ij})}{d\theta_{ij}} \geq 0$ and $\frac{du_i(\theta_{ij})}{d\theta_{ij}} \geq 0$, (b) $\theta^{min} u_i(\theta^{min}) - p_j(\theta^{min}) - M_{ij} \geq 0$, (c) $\frac{dp_j(\theta_{ij})}{d\theta_{ij}} = \theta_{ij} \cdot \frac{du_i(\theta_{ij})}{d\theta_{ij}}$.*

Proof. See Appendix B. □

Theorem 1 gives the necessary and sufficient conditions for a contract set Φ_i to be feasible. Therefore, each solution satisfying Theorem 1 guarantees that a UAV only accepts the contract designed for its own type, and provides the required transmit power to meet the downlink demand. Unfortunately, Theorem 1 results in a loose solution set, where an infinite number of feasible contracts exist. In order to continue the discussion, we will take the simplest solution, where $\frac{du_i(\theta_{ij})}{d\theta_{ij}} = \gamma_i > 0$, in the following analysis. Since the simplest contract is easy to implement, it is potential to be the best choice for practical uses. Note that, without loss of generality, other

solutions to Theorem 1 can be accommodated to the following approach as well. Consequently, the feasible contract that is proposed by BS i is given as follows.

Lemma 1. *Under the condition that $\frac{du_i(\theta_{ij})}{d\theta_{ij}} = \gamma_i$, the feasible contract between BS i and a UAV j of type θ_{ij} is $\phi_{ij} = (u_i, p_j) = (\gamma_i\theta_{ij}, \gamma_i\theta_{ij}^2/2)$, where $\gamma_i = \frac{m\alpha^2T^2}{2d_i^2}$.*

Proof. Based on $\frac{du_i(\theta_{ij})}{d\theta_{ij}} = \gamma_i$ and condition (c) of Theorem 1, it is easy to see $u_i = \gamma_i\theta_{ij}$ and $p_j = \gamma_i\theta_{ij}^2/2$. Then, condition (a) holds naturally, and condition (b) becomes $\theta^{\min} \geq \sqrt{2M_{ij}/\gamma_i}$. Based on the definition of the UAV type, condition (b) is equivalent to $\gamma_i \geq 2m\alpha^2t_{ij}(T-t_{ij})/d_i^2$. Then, by maximizing the right side over $t_{ij} \in [0, T/2]$, we set $\gamma_i = \frac{m\alpha^2T^2}{2d_i^2}$ to ensure that the contract will be feasible for all UAVs with any type θ_{ij} in Θ . \square

Therefore, for each overloaded BS i , the designed contract is $(u_i, p_j) = (\gamma_i\theta_{ij}, \gamma_i\theta_{ij}^2/2)$ with $\gamma_i = \frac{m\alpha^2T^2}{2d_i^2}$ for each UAV in \mathcal{J} with any type $\theta_{ij} \in \Theta$.

B. The optimal UAV association under the feasible contract

Given the feasible contract set $\{(\gamma_i\theta_{ij}, \gamma_i\theta_{ij}^2/2) | \forall \theta_{ij}\}$, the utility $R_{ij}(\theta_{ij})$ of each candidate UAV $j \in \mathcal{J}$ and the utility $U_{ij}(\theta_{ij})$ of the requesting BS i can be jointly determined. Then, the optimization problem in (12) becomes

$$\max_{j \in \mathcal{J}} U_{ij}(\theta_{ij}), \quad (21a)$$

$$\text{s. t. } p_{ij}(\mathbf{x}_{ij}^*, \rho_i^c) \leq p_j(\theta_{ij}) \leq \min\{p_{ij}^{\max}, p_{\max}\}, \quad (21b)$$

$$t_{ij} \leq T/2. \quad (21c)$$

Therefore, the last task is for BS i to find a UAV of the optimal type θ_{ij}^* that maximizes its utility in (21a), while satisfying the constraints (21b) and (21c). However, since BS i does not know the type or the movement duration of each UAV $j \in \mathcal{J}$, problem (21) is not solvable, until more information is provided to BS i . Therefore, during the association stage, after BS i sends the request signal with \mathbf{x}_{ij}^* , d_i , and Φ_i , each UAV j will respond with its type θ_{ij} . Ultimately, based on the responses, BS i can calculate the corresponding utility of each UAV, and employ the one that maximizes its own payoff. By substituting t_{ij} , u_i and p_j with θ_{ij} , we find that the derivation $\frac{dU_{ij}(\theta_{ij})}{d\theta_{ij}} < 0$. Therefore, the optimal UAV is $j^* = \arg \max_{j \in \mathcal{J}_i} U(\theta_{ij}) = \arg \min_{j \in \mathcal{J}_i} \theta_{ij}$, where $\mathcal{J}_i = \{j | p_{ij}(\mathbf{x}_{ij}^*, \rho_i^c) \leq \frac{\gamma_i}{2}\theta_{ij}^2 \leq \min\{p_{ij}^{\max}, p_{\max}\}, t_{ij} \leq T/2\}$. In other words, the qualified UAV with a smallest type will be the optimal solution. The complete process of the predictive UAV deployment process is summarized in Algorithm 1.

Algorithm 1 Proposed process for the UAV predictive deployment

For each BS $i \in \mathcal{I}$, once downlink communication exceeds the network capacity, **do**:

1. Learning stage:

- (a) BS i collects \mathcal{S}_i to model the UE distribution $f_i(\mathbf{y})$, estimate the downlink traffic density $S_i(\mathbf{y})$, and detect the hotspot area \mathcal{A}_i^c based on the WEM approaches proposed in Section IV.
- (b) BS i calculates the downlink demand d_i of the offloaded UEs via (6), estimates the number of required UAVs through (7), and computes the service point \mathbf{x}_{ij}^* for each target UAV j , based on the solution in [11].

2. Association stage:

- (a) BS i listens to the broadcast channel. If the channel is occupied, wait; Otherwise, BS i broadcasts the request signal with d_i , \mathbf{x}_{ij}^* , and $\Phi_i = \{\gamma_i \theta_{ij}, \frac{\gamma_i}{2} \theta_{ij}^2 | \forall \theta_{ij}\}$, where $\gamma_i = \frac{m\alpha^2 T^2}{2d_i^2}$.
- (b) Each UAV $j \in \mathcal{J}$ listens the broadcast channel. After receiving the request from BS i , each UAV calculates the movement time t_{ij} , its UAV type θ_{ij} with respect to BS i , and the available transmit power p_{ij}^{\max} after arriving at \mathbf{x}_{ij}^* . If $p_{ij}^{\max} \geq \frac{\gamma_i}{2} \theta_{ij}^2$ and $t_{ij} \leq T/2$, UAV j replies t_{ij} to BS i ; Otherwise, ignore.
- (c) BS i calculates the type θ_{ij} of each responding UAV j , finds the UAV set \mathcal{J}_i , and then, chooses the optimal UAV $j^* = \arg \min_{j \in \mathcal{J}_i} \theta_{ij}$.
- (d) BS i broadcasts the employment information and, then, releases the channel.

3. Movement stage: The employed UAV j^* starts to move towards the service point of the requesting BS i .

4. Service stage:

- (a) BS i pays $\gamma_i \theta_{ij^*} d_i$, and offloads the UEs within \mathcal{A}_i^c to UAV j^* .
- (b) UAV j^* provides the downlink service with a transmit power $p_{j^*} = \frac{\gamma_i}{2} \theta_{ij^*}^2$ for a service time $T - t_{ij^*}$.

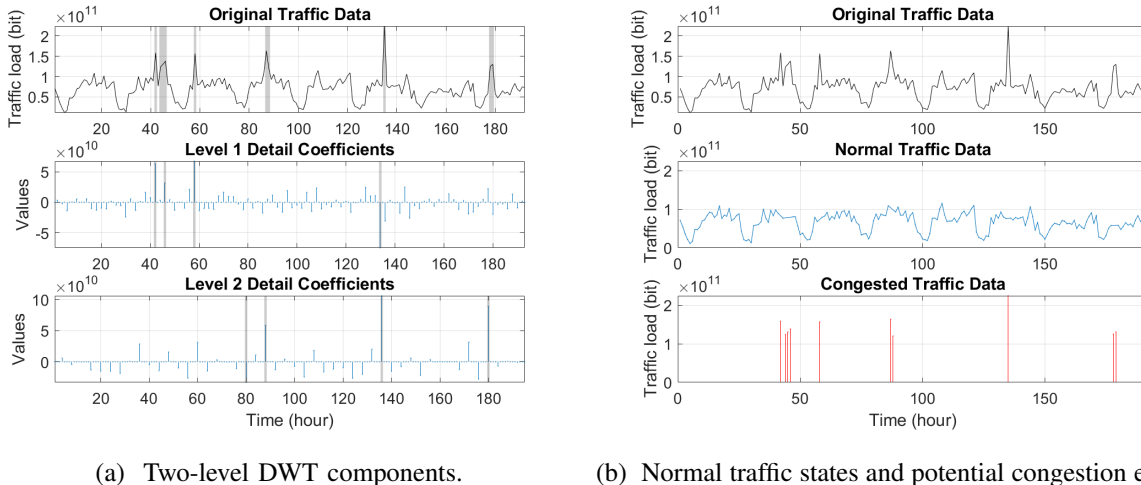
End

When the service stage ends, the BS-UAV association terminates. Then, UAV j^* starts to listen to the broadcast channel, or moves to a recharging station if its on-board energy E_j is low.

VI. NUMERIC RESULTS AND ANALYSIS

A. Simulation parameters

For our simulations, we consider a UAV-assisted wireless network in a dense urban environment, operating at the 2 GHz frequency with a downlink bandwidth of 20 MHz. The parameters in the LOS probability model are $a = 9.6$ and $b = 0.28$ [28]. The Gaussian parameters of the additional air-to-ground path loss are $\mu_{\text{LOS}} = 1.6$ and $\sigma_{\text{LOS}} = 8.41$ for the LOS link while $\mu_{\text{NLOS}} = 23$ and $\sigma_{\text{NLOS}} = 33.78$ for the NLOS case [27]. For the UAV parameters [35], we set the mobility power $m = 40$ W with an average moving speed of 5 m/s, and the hovering power is $p_h = 30$ W. For each UAV, the maximal on-board energy is 40 Wh, the recharging time is 10



(a) Two-level DWT components.

(b) Normal traffic states and potential congestion events.

Fig. 3: Two-level DWT is applied to detect the cellular traffic congestion from a city level.

minutes, and battery recharge can be finished at a closest BS³. The maximum downlink transmit power of a UAV aerial BS is $p_{\max} = 40$ W, and the unit cost of UAV’s on-board energy is $\alpha = 1$. At each UE, the average noise power spectral density is -174 dBm/Hz, and the price that UEs pays per bit of data is $\beta = 10e - 7$. For the UAV deployment process, we set $\Delta T = 1$ second, and the learning duration $\tau = 2$ minutes. The ratio of efficient transmission in each time slot is $\eta = 90\%$. Moreover, considering network congestion in a wireless cellular system lasts from a thousand seconds up to hours [36], we set T to be 18 minutes (1080 seconds), so that the offload service interval is shorter than the time period of common hotspot events.

B. Dataset description and preprocessing

An open-source dataset “city-cellular-traffic-map” in [24] is used for the modeling, training, and testing of the proposed UAV deployment framework. The dataset collects HTTP traffic data through the cellular networks during each hour within a middle-sized city of China from August 19 to August 26, 2012. The dataset consist of two parts. One lists the identification number (ID) and the location in longitude and latitude of each BS in the city, and the other collects the number of UEs, packets and traffic data (in bytes) that each BS transmits to downlink UEs during each hour of the aforementioned eight days.

In order to identify potential hotspot events in the dataset, we apply the discrete wavelet transform (DWT) to check the cellular traffic during each hour in the city level. As shown in the upper figure of Fig. 3, the cellular traffic within the city area presents a conspicuously periodic pattern, with several sudden and erratic surges. DWT processes the time-serial data by

³The energy-efficient trajectory optimization for UAV power recharge will be subject to our future work.

analyzing both the value and frequency component of each data point, where the lower-frequency component defines the long term trend of the data, and the higher-frequency component represents the small-scale rapid signal variation. A hotspot event usually causes a steep surge in a cellular traffic amount. Therefore, such rapid change can be captured by DWT in the higher frequency domain. As shown in Fig. 3a, a two-level DWT is applied to detect the frequency change of the cellular traffic, and the gray bars mark the time points when the traffic amount has a sudden increase. Based on the result, the dataset is separated into the normal traffic data and the potential congested traffic, as given in Fig. 3b. Here, we find a time window from 42 to 47, which is 18 to 23 p.m. on August 20, that shows a continuously high cellular traffic amount, and the hotspot event is highly likely to happen in the city during this period. Therefore, the traffic data from 42 to 47 are selected to study the predictive UAV deployment in the following analysis.

However, the data in [24] does not include the location information of each connected UE, or the service area of each BS. In order to identify the UE distribution and the downlink traffic density, the location and time labels are generated and attached to each downlink transmission record via the following approach. First, the service area \mathcal{A}_i of each BS i is partitioned, based on the closest-distance principle. Next, we use the total packet number to denote the number of downlink transmissions. Furthermore, we note that the original time label t is based on one hour, which is too coarse to enable our analysis. Therefore, a new label with a finer time grain of one second is randomly generated and attached to each traffic record. Eventually, the location label \mathbf{y}_n of each traffic record is generated by a GMM with random parameters to which we add a zero-mean Gaussian noise. The variance of the Gaussian noise is set as three meters, which is the average error of the GPS location for common mobile equipments. With the additional location and time information, the dataset is suitable for the studied problem.

C. Performance of the cellular traffic prediction

Given that $T = 18$ and $\tau = 2$, in the learning approach, each overloaded BS i will take two minutes to collect the transmission records \mathcal{S}_i , and predict the total data demand d_i for the next eighteen minutes. In order to guarantee that the training dataset \mathcal{S}_i is representative, we assume that each UE will have at least one downlink transmission during the learning stage. This assumption is supported by the analysis result in Fig. 4, which shows that over 70% UEs receive, on average, one packet within every two minutes. Based on the collected dataset \mathcal{S}_i , the proposed WEM approach is applied to predict the data demand d_i within the hotspot area \mathcal{A}_i^c ,

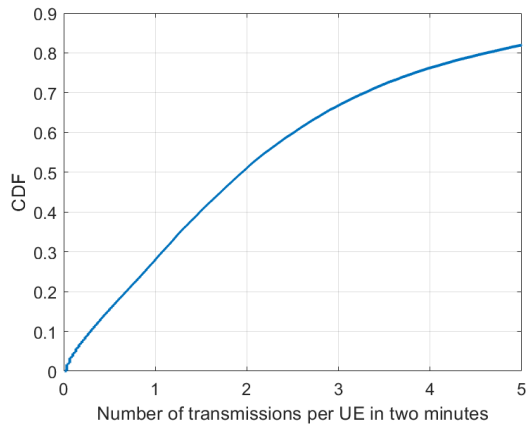


Fig. 4: CDF of the number of transmissions per UE per two minutes.

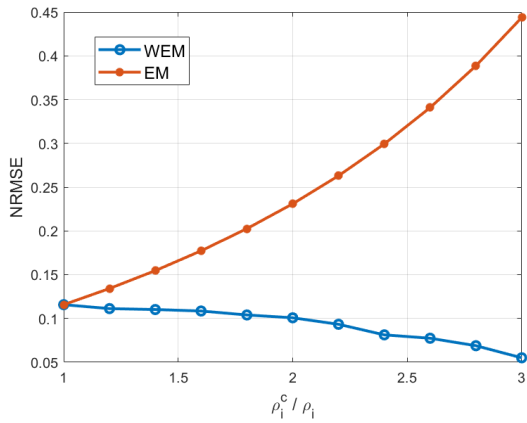
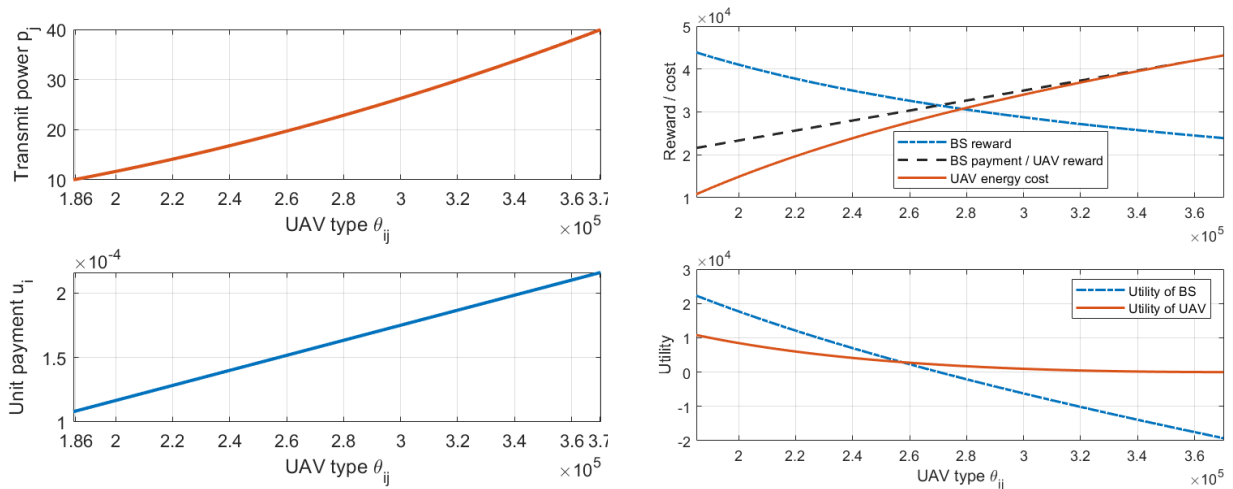


Fig. 5: NRMSE of the proposed WEM approach and the baseline EM method.

while the actual traffic demand d_i^{actual} is calculated by summing up the real transmission amount within \mathcal{A}_i^c during the following T . In order to evaluate the performance of the proposed WEM method, the normalized root mean-squared error (NRMSE) of the traffic prediction is defined as $\delta_{\text{NRMSE}} = \sqrt{\mathbb{E}_{i,t}[(\frac{d_i - d_i^{\text{actual}}}{d_i^{\text{actual}}})^2]}$. For comparison purposes, we use the EM approach as a baseline to evaluate the prediction accuracy of our solution. Note that, the EM method has been used in Section IV-A for modeling the UE distribution $f_i(\mathbf{y})$. Then, the predicted traffic demand resulting from the EM method will be $d_i^{\text{EM}} = T \cdot \mathbb{E}_n(s_n) \cdot \int_{\mathbf{y} \in \mathcal{A}_i^c} f_i(\mathbf{y}) d\mathbf{y}$, where $\mathbb{E}_n(s_n) = \frac{\sum_n s_n \Delta t}{\tau}$ is the time average of the summed data rate towards all UEs, and $\int_{\mathbf{y} \in \mathcal{A}_i^c} f_i(\mathbf{y}) d\mathbf{y}$ is the percentage of UEs within the hotspot area. We repeat the simulation for 1000 times. In each run, the location and time labels of each transmission record are generated randomly.

Fig. 5 shows the NRMSE resulting from the WEM and EM methods in predicting the downlink demand, as the average data demand ρ_i^c of the hotspot UEs increases. When $\frac{\rho_i^c}{\rho_i}$ equals to one, each hotspot UE will have the same data demand as the other UEs in the service area \mathcal{A}_i . In this case, the WEM and EM approaches yield a similar prediction accuracy with an NRMSE



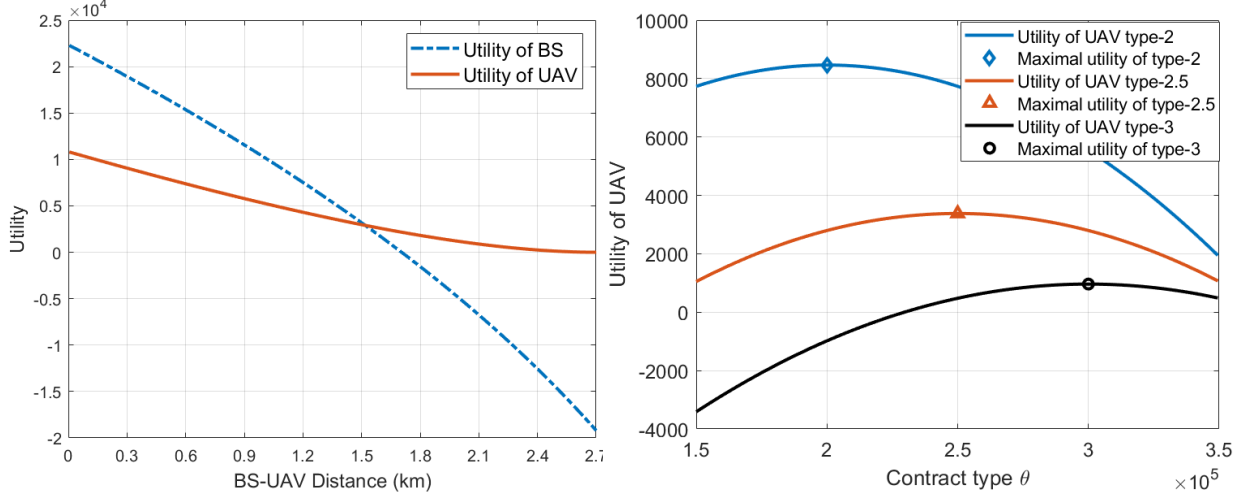
(a) Transmit power and unit payment, given different UAV types. (b) Costs, rewards and overall utilities of the associated BS and UAV, given different UAV types.

Fig. 6: As the UAV type increases, the transmit power and the unit payment both increase. However, the overall utilities of the associated BS and UAV will decrease.

of 12%. The prediction error of 12% yields lower than 0.1 W of deviation on the value of $p_{ij}(\mathbf{x}_{ij}^*, \rho_i)$. Clearly, this is a very small value compared to the hovering and transmit powers of a typical UAV. When the traffic load within different regions of the cellular network becomes more uneven, the performance of the WEM and EM methods will vary differently. When the traffic density of the hotspot region increases to the triple of the network average, the prediction error of WEM decreases from 12% to 5%, while the EM error increases from 12% to 45%. In the proposed WEM approach, the traffic density $\bar{S}_i(\mathbf{y})$ of each location \mathbf{y} is considered when optimizing the parameters of the prediction model. Therefore, the spatial feature of downlink transmissions can be accurately captured, and the performance of WEM becomes better, as the traffic load in the cellular system becomes uneven. However, the EM model only considers the location information, but ignores the downlink rate of each transmission. Therefore, when the traffic demand shows distinct patterns in different regions, the EM method fails to capture the spatial diversity. As a result, the performance of the EM method will decrease significantly, as the cellular traffic load becomes more uneven.

D. Performance of the designed contracts

In this section, we study the performance of the designed contract by evaluating the individual utilities of a BS and its associated UAV. The contract is designed based on Lemma 1 by a BS with ID 7939, using the data from time 42 in [24]. Fig. 6a shows the relationship between the



(a) Utilities of BS and UAV, given different distances. (b) Utilities of UAVs, given different contract types.

Fig. 7: The designed contract ensures the employed UAV to receive a non-negative payoff, and the highest utility is achieved by accepting the contract of its own type.

type of the associated UAV with the transmit power and the unit payment in the contract. As the UAV type θ_{ij} increases, both the transmit power p_j and the unit payment u_i in the contract will increase. This result supports the conclusion of Proposition 1, where a UAV of a higher type is required to provide more transmit power and will be given a higher unit payment. Fig. 6b investigates the relationship between the UAV type and the reward, cost, as well as the overall utilities of the requesting BS and the deployed UAV, respectively. First, as the UAV type θ_{ij} becomes larger, although the transmit power $p_j(\theta_{ij})$ increases, the BS's reward $\beta B_{ij}(p_j)$ from the downlink UEs will decrease. Note that, given the downlink demand d_i fixed, a higher UAV type θ_{ij} results in a longer travel time t_{ij} . By substituting t_{ij} with θ_{ij} in (8), we find that the derivation $\frac{dB_{ij}(\theta_{ij})}{d\theta_{ij}} < 0$. Therefore, the BS's reward $\beta B_{ij}(\theta_{ij})$ will decrease as the UAV type θ_{ij} increases. Moreover, as shown in Fig. 6b, a higher UAV type results in a higher payment $u_i(\theta_{ij})d_i$ from BS i to UAV j . Therefore, the utility of BS i will be lower for a larger θ_{ij} . For the deployed UAV j , a larger type θ_{ij} leads to a higher reward $u_i(\theta_{ij})d_i$ from BS i , but meanwhile, the energy cost will increase, due to a longer movement time t_{ij} and a higher transmit power p_i . Furthermore, as shown in Fig. 6b, the energy cost increases faster than the economic benefit. Thus, the utility of the deployed UAV will also decrease, as θ_{ij} becomes larger.

Next, we study the relationship between the BS-UAV distance and the individual utilities of the BS and its associated UAV. As shown in Fig. 7a, if the distance between a BS and its employed UAV becomes larger, the utilities of the UAV and the BS will both decrease, because a longer BS-UAV distance results in a larger movement time t_{ij} and a higher UAV type θ_{ij} . Since

the unit payment $u_i(\theta_{ij})$ of the BS will increase to compensate for the UAV's mobility power over the longer distance, the utility of BS i becomes negative, when the distance is larger than 1.7 km. On the other hand, for the employed UAV, as the movement distance becomes larger, more power will be consumed during the movement stage and more transmit power is required during the service stage. Therefore, the utility of UAV decreases with the increase of the moving distance. However, due to the IR condition, the payment from the BS will increase accordingly. Fig. 7a shows that the UAV's utility is always non-negative. Therefore, we can conclude that the IR condition holds in the designed contract in Lemma 1. Fig. 7b investigates how the IC condition holds in the designed contract. The utilities of three UAVs, where their actual types are 2×10^5 (type-2), 2.5×10^5 (type-2.5), and 3×10^5 (type-3), is shown in Fig. 7b, when they accept different kinds of contracts from BS 7939. As shown in Fig. 7b, the maximum utility of each UAV is achieved when the accepted contract is of its own type. Therefore, the IC condition holds, and the designed contract set of Lemma 1 is feasible.

An interesting observation on the utility function is that the prediction error of d_i does not cause small fluctuations on the utility value of the BS or the employed UAV. Although d_i determines the type θ_{ij} of each UAV and the value of γ_i , after expanding the expressions of utility functions, we find that the transmit power is $p_j = \gamma_i \theta_{ij}^2 / 2 = \frac{mT^2}{4\alpha(T-t_{ij})^2}$ and the total payment from BS i to the employed UAV j is $u_i d_i = \gamma_i \theta_{ij} d_i = \frac{mT^2}{2(T-t_{ij})}$. Therefore, d_i no longer appears in the formulas, and an inaccuracy in d_i will not impact the utility functions in (9) and (10). The main effect of d_i in the predictive UAV deployment is to determine the minimum required transmit power $p_{ij}(\mathbf{x}_{ij}^*, \rho_i^c)$. If the predicted demand d_i is much lower than the real data demand, then $p_{ij}(\mathbf{x}_{ij}^*, \rho_i^c)$ will be smaller. In consequence, some UAVs without enough energy may be inappropriately considered to be a qualified choice, and might be employed. On the other hand, if d_i is much higher than the actual demand, some qualified UAVs with enough power may be excluded from the candidate set \mathcal{J}_i . Both cases can lead to a suboptimal solution to (12). However, as long as the error on d_i causes no change to the association result, the utilities of BS i and the employed UAV will always be accurate. Based on this observation, the proposed approach is highly robust to prediction errors.

E. Evaluation of the predictive UAV deployment

In Fig. 8, we evaluate the performance of the proposed UAV deployment method, by comparing it with an event-driven allocation approach, which requests the closest UAV every time the

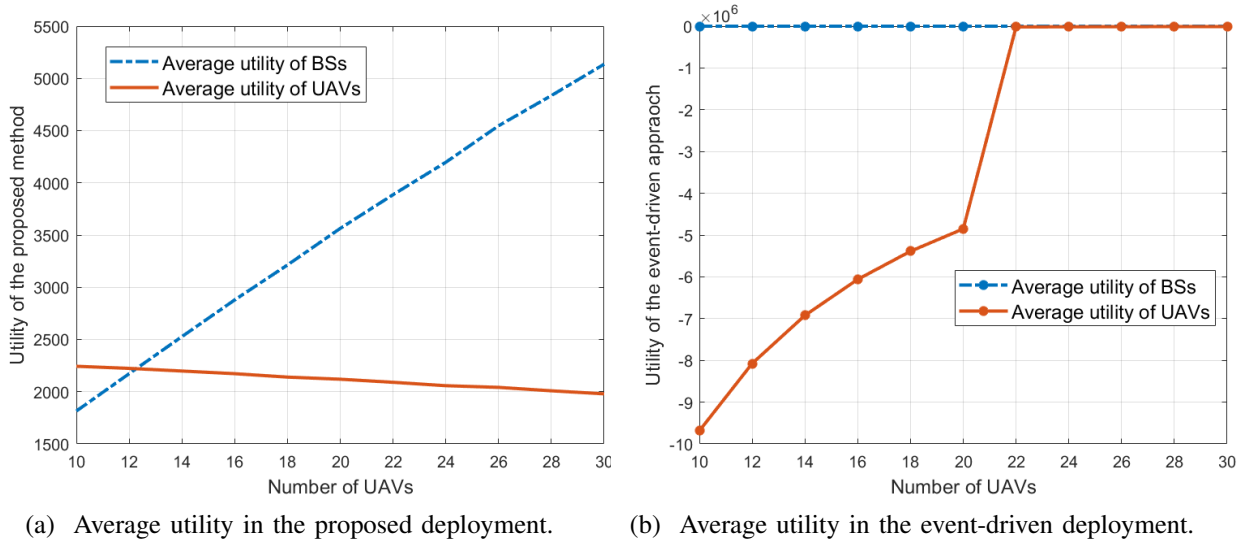


Fig. 8: Average utilities of BSs and UAVs, given different numbers of available UAVs in the network.

downlink congestion occurs, without the prediction on traffic demand or the feasible contract design. In the event-driven approach, the unit payment u_i from BS i to the employed UAV equals to the unit price β from downlink UEs. In return, the employed UAV j provides the downlink service to the best of its power ability, where $p_j = \min\{p_{ij}(\mathbf{x}_{ij}^*, \rho_i), p_{ij}^{\max}, p_{\max}\}$. The traffic data from time 42 to 43 in [24] is used to evaluate the performance of two approaches. We repeat the simulation for 1000 times. In each run, the initial location and on-board energy of each UAV, as well as the location and time label of each transmission record, are generated randomly.

First, Fig. 8a shows that the average utilities of both the overloaded BSs and the employed UAVs, resulting from the proposed approach, will be positive. As the number of available UAVs increases, each overloaded BS have more options to offload its excess downlink traffic and maximize its utility. Thus, the average utility of each BS will increase, given more available UAVs. On the other hand, since the number of overloaded BSs is around 21, the number of employed UAVs will be fixed near 21. In consequence, as more UAVs is available, the average utility of each UAV naturally decreases. However, the total utility of all UAVs becomes larger. Given more UAVs distributed in the network, the average distance between each overloaded BS and its employed UAV will decrease. Therefore, less energy is consumed during the movement stage, and the aerial cellular service can be provided to the UEs with a shorter delay. In consequence, the total utility of the BS and UAV groups both increase in the proposed deployment method, as the number of available UAVs increases. However, in the event-driven method, as shown in Fig. 8b, the average utility of each overloaded BS is always zero, and the utility of each UAV is negative. Since each BS gives all its income from downlink UEs to the employed UAV,

the utility of each BS is always zero. On the other hand, without a proper prediction on the UE distribution and traffic demand, the employed UAV in the event-driven approach must change its location constantly to meet the on-demand transmission need. Therefore, a lot of energy will be consumed by mobility, and the overall utility for each UAV is always negative. Furthermore, given the number of overloaded BSs is around 21, the average utility of each UAV increases dramatically, when the number of UAVs changes from 20 to 22. When the number of UAVs is smaller than BSs, the travel distance of each UAV to the associated BS is usually large, and a lot of energy is consumed during the mobility stage. Although each BS gives all the payment from UEs to the employed UAV, in the most cases, the payment cannot offset the energy cost of each UAV. As the number of UAVs is greater than BSs, such problem becomes less serious. However, the average utility of each UAV is still negative.

From Fig. 8, we can conclude that, the event-driven approach fails to be a practical solution to the considered UAV deployment problem, because the negative revenue will discourage UAV operators from providing aerial cellular service. However, in the proposed UAV deployment approach, due to the designed contract, a sufficient payment is provided to the employed UAV to reward its aerial cellular service, and the downlink data demand within the hotspot area can be satisfied. Therefore, both the BS and UAV operators can receive positive revenues. Furthermore, simulation results show that the UAV's recharging frequency in the proposed approach is around 50% higher than the event-driven method. Therefore, the proposed approach enables each UAV to use its on-board energy more efficiently to serve the hotspot UEs with downlink communications, and shows a significant advantage on the economical revenues of both the BS and UAV networks, compared with the baseline, event-driven approach.

VII. CONCLUSION

In this paper, we have proposed a novel approach for predictive deployment of UAV base stations to complement the ground cellular system in face of the hotspot events. In particular, four inter-related and sequential stages have been proposed to enable the ground BS to optimally employ a UAV to offload the excess downlink traffic. First, a novel framework, based on the EM and WEM methods, has been proposed to estimate the UE distribution and the downlink traffic demand. Next, to guarantee a truthful information exchange between the BS and UAV operators, a traffic offload contract have been developed, and the sufficient and necessary conditions for having a feasible contract have been analytically derived. Then, an optimization problem have

been formulated to deploy the optimal UAV onto the hotspot area in a way that the utility of each overloaded ground BS is maximized. Simulation and analytical results show that the proposed WEM approach yields a prediction error which is lower than 12%, and compared with a conventional EM approach, the WEM method yields a significant advantage on the prediction accuracy, as the traffic load in the cellular system becomes spatially uneven. Furthermore, compared with a baseline, event-driven allocation method, the proposed predictive deployment approach enables UAV operators to provide efficient downlink service for hotspot users, and significantly improves the revenues of both the BS and UAV networks.

APPENDIX A

PROOF OF PROPOSITION 1

We first use contradiction to prove the proposition that if $\theta_{ij} > \theta'_{ij}$, then $u_i(\theta_{ij}) \geq u_i(\theta'_{ij})$. Then, we prove that if $u_i(\theta_{ij}) \geq u_i(\theta'_{ij})$, then $p_j(\theta_{ij}) \geq p_j(\theta'_{ij})$. Suppose that there exists $u_i(\theta_{ij}) < u_i(\theta'_{ij})$, but $\theta_{ij} > \theta'_{ij}$. Then, we have

$$\theta_{ij}u_i(\theta'_{ij}) + \theta'_{ij}u_i(\theta_{ij}) > \theta_{ij}u_i(\theta_{ij}) + \theta'_{ij}u_i(\theta'_{ij}). \quad (22)$$

On the other hand, from IC condition, we have

$$\theta_{ij}u_i(\theta_{ij}) - p_j(\theta_{ij}) \geq \theta_{ij}u_i(\theta'_{ij}) - p_j(\theta'_{ij}), \quad \theta'_{ij}u_i(\theta'_{ij}) - p_j(\theta'_{ij}) \geq \theta'_{ij}u_i(\theta_{ij}) - p_j(\theta_{ij}). \quad (23)$$

By adding the inequations in (23), we have $\theta_{ij}u_i(\theta_{ij}) + \theta'_{ij}u_i(\theta'_{ij}) \geq \theta_{ij}u_i(\theta'_{ij}) + \theta'_{ij}u_i(\theta_{ij})$, which contradicts to (22). This completes the first part of the proof.

Next, we prove that if $u_i(\theta_{ij}) \geq u_i(\theta'_{ij})$, $p_j(\theta_{ij}) \geq p_j(\theta'_{ij})$. From the IC condition, we have

$$\theta'_{ij}u_i(\theta'_{ij}) - p_j(\theta'_{ij}) \geq \theta'_{ij}u_i(\theta_{ij}) - p_j(\theta_{ij}), \quad (24)$$

i.e. $p_j(\theta_{ij}) - p_j(\theta'_{ij}) \geq \theta'_{ij} (u_i(\theta_{ij}) - u_i(\theta'_{ij}))$. Since $u_i(\theta_{ij}) > u_i(\theta'_{ij})$, we conclude

$$p_j(\theta_{ij}) - p_j(\theta'_{ij}) \geq \theta'_{ij} (u_i(\theta_{ij}) - u_i(\theta'_{ij})) \geq 0, \quad (25)$$

and thus $p_j(\theta_{ij}) \geq p_j(\theta'_{ij})$. This completes the proof.

APPENDIX B

PROOF OF THEOREM 1

For notational simplicity, we omit the subscript of variables u_i , p_j , θ_{ij} , M_{ij} , and denote them as u , P , θ , M respectively.

A. Proof for necessary conditions

Given the IR and IC conditions, we prove Theorem 1 in this section. First, as shown in Proposition 1, for any $\theta, \theta' \in \Theta$, once $\theta > \theta'$, then $u(\theta) \geq u(\theta')$ and $P(\theta) \geq P(\theta')$. Therefore, condition (a) of Theorem 1 is proved by Proposition 1. Second, condition (b) of Theorem 1 is supported by the IR condition, where $R_{ij}(\theta) \geq 0$ for all θ in Θ , which naturally includes θ^{\min} . Next, we prove condition (c). Let $\Delta\theta = \theta' - \theta$. According to the IC condition, for any $\Delta\theta \in [\theta^{\min} - \theta^{\max}, 0) \cup (0, \theta^{\max} - \theta^{\min}]$, we have: $\theta \cdot u(\theta) - P(\theta) \geq \theta \cdot u(\theta + \Delta\theta) - P(\theta + \Delta\theta)$, i.e., $\theta \cdot [u(\theta) - u(\theta + \Delta\theta)] \geq P(\theta) - P(\theta + \Delta\theta)$. If $\Delta\theta > 0$, then according to Proposition 1, $u(\theta + \Delta\theta) \geq u(\theta)$ and $P(\theta + \Delta\theta) \geq P(\theta)$. Here, we exclude the situation where $u(\theta + \Delta\theta) = u(\theta)$ and $P(\theta + \Delta\theta) = P(\theta)$ in the following discussion of this proof, because condition (c) naturally holds in this case. Therefore, for any $\Delta\theta \in (0, \theta^{\max} - \theta^{\min}]$, we have

$$\theta \leq \frac{P(\theta + \Delta\theta) - P(\theta)}{u(\theta + \Delta\theta) - u(\theta)}. \quad (26)$$

If $\Delta\theta < 0$, then $u(\theta + \Delta\theta) < u(\theta)$ and $P(\theta + \Delta\theta) < P(\theta)$. Thus, for any $\Delta\theta \in [\theta^{\min} - \theta^{\max}, 0)$,

$$\theta \geq \frac{P(\theta + \Delta\theta) - P(\theta)}{u(\theta + \Delta\theta) - u(\theta)}. \quad (27)$$

Consequently, by combing (26) and (27) and letting $\Delta\theta \rightarrow 0$, we have

$$\frac{dP}{d\theta} / \frac{du}{d\theta} = \lim_{\Delta\theta \rightarrow 0} \frac{P(\theta + \Delta\theta) - P(\theta)}{u(\theta + \Delta\theta) - u(\theta)} = \theta, \quad (28)$$

which proves condition (c) of Theorem 1.

B. Proof for sufficient conditions

From Theorem 1, we will prove the IR and IC conditions in this section. First, we prove the IR condition. According to condition (b) of Theorem 1, θ^{\min} satisfies the IR condition. Then, we prove that for any $\theta \in (\theta^{\min}, \theta^{\max}]$, the IR condition holds. From condition (c) of Theorem 1, we have the following inequalities, $\frac{P(\theta) - P(\theta^{\min})}{u(\theta) - u(\theta^{\min})} \leq \theta$, i.e.,

$$P(\theta^{\min}) \geq P(\theta) - \theta \cdot [u(\theta) - u(\theta^{\min})]. \quad (29)$$

From condition (b), we have

$$\theta^{\min} \cdot u(\theta^{\min}) - P(\theta^{\min}) - M \geq 0. \quad (30)$$

By combing (29) and (30), we have $\theta \cdot u(\theta) - P(\theta) - M \geq (\theta - \theta^{\min}) \cdot u(\theta^{\min}) \geq 0$. Thus, for any $\theta \in \Theta$, the IR condition holds.

In the end, we prove the IC condition. Let $h = \theta \cdot u(\theta) - P(\theta) - M - [\theta \cdot u(\theta') - P(\theta') - M]$. And we prove that $h \geq 0$. From condition (c), we have, if $\theta' > \theta$, then

$$\frac{P(\theta') - P(\theta)}{u(\theta') - u(\theta)} \geq \min\{\theta, \theta'\} = \theta. \quad (31)$$

i.e., $P(\theta') - P(\theta) \geq \theta \cdot [u(\theta') - u(\theta)]$. Therefore, $h = \theta \cdot [u(\theta) - u(\theta')] + P(\theta') - P(\theta) \geq 0$. On the other hand, if $\theta' < \theta$, then

$$\frac{P(\theta) - P(\theta')}{u(\theta) - u(\theta')} \leq \max\{\theta, \theta'\} = \theta. \quad (32)$$

i.e., $P(\theta) - P(\theta') \leq \theta \cdot [u(\theta) - u(\theta')]$. Therefore, $h \geq 0$. Consequently, the IC condition holds.

REFERENCES

- [1] Q. Zhang, M. Mozaffari, W. Saad, M. Bennis, and M. Debbah, "Machine learning for predictive on-demand deployment of UAVs for wireless communications," in *Proc. of IEEE Global Communications Conference*, Abu Dhabi, UAE, Dec 2018.
- [2] M. Mozaffari, W. Saad, M. Bennis, and M. Debbah, "Mobile unmanned aerial vehicles (UAVs) for energy-efficient internet of things communications," *IEEE Transactions on Wireless Communications*, vol. 16, no. 11, pp. 7574–7589, Sep 2017.
- [3] R. I. Bor-Yaliniz, A. El-Keyi, and H. Yanikomeroglu, "Efficient 3-D placement of an aerial base station in next generation cellular networks," in *Proc. of IEEE International Conference on Communications*, Kuala Lumpur, Malaysia, May 2016.
- [4] X. Zhang and L. Duan, "Fast deployment of UAV networks for optimal wireless coverage," *IEEE Transactions on Mobile Computing*, vol. 18, no. 3, pp. 588–601, May 2018.
- [5] W. Khawaja, I. Guvenc, D. Matolak, U.-C. Fiebig, and N. Schneckenberger, "A survey of air-to-ground propagation channel modeling for unmanned aerial vehicles," *IEEE Communications Surveys and Tutorials (Early Access)*, May 2019.
- [6] M. Mozaffari, W. Saad, M. Bennis, Y.-H. Nam, and M. Debbah, "A tutorial on UAVs for wireless networks: Applications, challenges, and open problems," *IEEE Communications Surveys and Tutorials*, to appear, 2019.
- [7] M. Mozaffari, A. T. Z. Kasgari, W. Saad, M. Bennis, and M. Debbah, "Beyond 5G with UAVs: Foundations of a 3D wireless cellular network," *IEEE Transactions on Wireless Communications*, vol. 18, no. 1, pp. 357–372, Jan 2018.
- [8] W. Saad, M. Bennis, and M. Chen, "A vision of 6G wireless systems: Applications, trends, technologies, and open research problems," *IEEE Network*, to appear, 2019.
- [9] M. Chen, U. Challita, W. Saad, C. Yin, and M. Debbah, "Artificial neural networks-based machine learning for wireless networks: A tutorial," *IEEE Communications Surveys and Tutorials*, to appear, 2019.
- [10] Z. Hu, Z. Zheng, L. Song, T. Wang, and X. Li, "UAV offloading: Spectrum trading contract design for UAV assisted cellular networks," *IEEE Transactions on Wireless Communications*, vol. 17, no. 9, pp. 6093–6107, July 2018.
- [11] M. Mozaffari, W. Saad, M. Bennis, and M. Debbah, "Optimal transport theory for power-efficient deployment of unmanned aerial vehicles," in *Proc. of IEEE International Conference on Communications*, Kuala Lumpur, Malaysia, May 2016.
- [12] E. Kalantari, H. Yanikomeroglu, and A. Yongacoglu, "On the number and 3D placement of drone base stations in wireless cellular networks," in *Proc. of IEEE 84th Vehicular Technology Conference*, Montreal, QC, Canada, Sep 2016.
- [13] J. Lyu, Y. Zeng, and R. Zhang, "UAV-aided offloading for cellular hotspot," *IEEE Transactions on Wireless Communications*, vol. 17, no. 6, pp. 3988–4001, Mar 2018.
- [14] V. Sharma, M. Bennis, and R. Kumar, "UAV-assisted heterogeneous networks for capacity enhancement," *IEEE Communications Letters*, vol. 20, no. 6, pp. 1207–1210, Apr 2016.

- [15] J. Lyu, Y. Zeng, and R. Zhang, "Spectrum sharing and cyclical multiple access in UAV-aided cellular offloading," in *Proc. of IEEE Global Communications Conference*, Singapore, Dec 2017.
- [16] F. Cheng, S. Zhang, Z. Li, Y. Chen, N. Zhao, R. Yu, and V. C. Leung, "UAV trajectory optimization for data offloading at the edge of multiple cells," *IEEE Transactions on Vehicular Technology*, vol. 67, no. 7, pp. 6732 – 6736, Mar 2018.
- [17] S. Sharafeddine and R. Islambouli, "On-demand deployment of multiple aerial base stations for traffic offloading and network recovery," *arXiv preprint arXiv:1807.02009*, 2018.
- [18] R. Li, Z. Zhao, J. Zheng, C. Mei, Y. Cai, and H. Zhang, "The learning and prediction of application-level traffic data in cellular networks," *IEEE Transactions on Wireless Communications*, vol. 16, no. 6, pp. 3899–3912, Mar 2017.
- [19] C. Yu, Y. Liu, D. Yao, L. T. Yang, H. Jin, H. Chen, and Q. Ding, "Modeling user activity patterns for next-place prediction," *IEEE Systems Journal*, vol. 11, no. 2, pp. 1060–1071, July 2017.
- [20] P. Valente Klaine, M. A. Imran, O. Onireti, and R. D. Souza, "A survey of machine learning techniques applied to self organizing cellular networks," *IEEE Communications Surveys and Tutorials*, vol. 19, no. 4, pp. 2392–2431, July 2017.
- [21] M. Chen, W. Saad, and C. Yin, "Liquid state machine learning for resource and cache management in LTE-U unmanned aerial vehicle (UAV) networks," *arXiv preprint arXiv:1801.09339*, 2018.
- [22] J. Chen, U. Yatnalli, and D. Gesbert, "Learning radio maps for UAV-aided wireless networks: A segmented regression approach," in *Proc. of IEEE International Conference on Communications*, Paris, France, May 2017.
- [23] R. Amorim, J. Wigard, H. Nguyen, I. Z. Kovacs, and P. Mogensen, "Machine-learning identification of airborne UAV-UEs based on LTE radio measurements," in *Proc. of IEEE Globecom Workshops*, Singapore, Jan 2017.
- [24] "City cellular traffic map," <https://github.com/caesar0301/city-cellular-traffic-map>, accessed: 2016-10-05.
- [25] P. Bolton and M. Dewatripont, *Contract theory*. MIT press, 2005.
- [26] L. Zhu, J. Zhang, Z. Xiao, X. Cao, D. O. Wu, and X.-G. Xia, "3D beamforming for flexible coverage in millimeter-wave uav communications," *IEEE Wireless Communications Letters*, 2019.
- [27] A. Al-Hourani, S. Kandeepan, and A. Jamalipour, "Modeling air-to-ground path loss for low altitude platforms in urban environments," in *Proc. of IEEE Global Communications Conference*, Austin, TX, USA, Dec 2014.
- [28] A. Al-Hourani, S. Kandeepan, and S. Lardner, "Optimal LAP altitude for maximum coverage," *IEEE Wireless Communications Letters*, vol. 3, no. 6, pp. 569–572, July 2014.
- [29] J. Lyu, Y. Zeng, and R. Zhang, "Cyclical multiple access in UAV-aided communications: A throughput-delay tradeoff," *IEEE Wireless Communications Letters*, vol. 5, no. 6, pp. 600–603, Aug 2016.
- [30] Y. Zeng, J. Xu, and R. Zhang, "Energy minimization for wireless communication with rotary-wing UAV," *IEEE Transactions on Wireless Communications*, vol. 18, no. 4, pp. 2329 – 2345, 2019.
- [31] B. L. Stevens, F. L. Lewis, and E. N. Johnson, *Aircraft control and simulation: dynamics, controls design, and autonomous systems*. John Wiley & Sons, 2015.
- [32] A. T. Z. Kasgari, W. Saad, and M. Debbah, "Human-in-the-loop wireless communications: Machine learning and brain-aware resource management," *IEEE Transactions on Communications*, to appear, 2019.
- [33] B. Selim, O. Alhusssein, S. Muhaidat, G. K. Karagiannidis, and J. Liang, "Modeling and analysis of wireless channels via the mixture of Gaussian distribution," *IEEE Transactions on Vehicular Technology*, vol. 65, no. 10, pp. 8309–8321, 2015.
- [34] M. B. Christopher, *Pattern recognition and machine learning*. Springer-Verlag New York, 2016.
- [35] "DJI matrice 200 series v2 specifications," <https://www.dji.com/downloads/products/matrice-200-series-v2>, accessed: 2019.
- [36] BITAG, "Real-time network management of internet congestion," *Broadband Internet Technical Advisory Group*, Oct 2013.